Published in "Chemical Communications 54(86): 12218–12221, 2018"
which should be cited to refer to this work.

Bimetallic metal organic frameworks with precisely positioned metal centers for efficient H_2 storage†

Daeok Kim,[a] Kyung Seob Song,[b] Onur Buyukcakir,[a] Taner Yildirim*[c] and Ali Coskun *[b]

We demonstrated that the ratio and position of two different metal ions, Pd and Cu, can be precisely controlled within MOFs through predesigned metal clusters. These MOF structures incorporating Pd–Cu paddle wheel units were synthesised simply by reacting Pd–Cu acetate metal clusters and tritopic organic linkers at room temperature. Pd–Cu open metal sites were found to be uniformly distributed throughout the MOFs with a *ca.* 1 : 1 ratio. The incorporation of Pd into the MOF structure also led to enhanced affinity towards H_2 with Q_{st} values up to 8.9 kJ mol^{-1}.

Metal–organic frameworks (MOFs) are crystalline porous materials composed of periodic and successive binding of either metal ions or metal oxide clusters with organic linkers.[1,2] The combinations of metals and organic linkers have already led to a great number of functional porous structures with specifically tailored functions towards gas storage & separation,[3–6] catalysis,[7–9] bio-applications,[10,11] sensors,[12–14] and so on.[15,16]

Recently, MOFs have also been explored as supports for metal and metal oxide nanoparticles to impart new functions such as enhanced gas affinity.[17–19] Among all the transition metals, Pd has been of considerable interest due to its versatile use in H_2 storage.[20–23] As a pioneering result in this particular area, Kaskel *et al.* had successfully infiltrated Pd nanoparticles into MOF-5 and achieved enhancement in H_2 storage.[20] Similarly, Suh and coworkers also reported enhanced hydrogen uptake capacities at 77 K and room temperature owing to the presence of Pd nanoparticles located in the pores of a redox-active MOF.[21] Latroche *et al.* demonstrated the incorporation of Pd nanoparticles (~2.0 nm) within the pores of the MIL-100(Al), compared to the pristine MOF.[22] This result was explained by the spillover mechanism in which H_2 dissociates at the surface of the Pd nanoparticles and the *in situ* formed atomic hydrogens diffuse into the pores of MOF. Despite these encouraging results, however, the Pd/MOF composites still present important challenges such as the decrease in pore volume and surface area due to the pore blocking by Pd nanoparticles along with their inhomogeneous dispersion and aggregation within MOFs.

Recently, Doonan and coworkers have elegantly reported on the synthesis of Pd/Zn, Pd/Cu, and Pd/Ni metal organic polyhedras using bimetallic paddle wheel acetates, thus demonstrating the possibility of using bimetallic clusters as pre-designed secondary building units for the synthesis of bimetallic porous materials.[24] Along this direction, Serre *et al.* have also demonstrated the usage of a multi-metal acetic acid complex as a precursor for the synthesis of multi-metal MOF structures.[25] We note that the immobilization of Pd single atoms in the form of open metal sites (OMSs) within the metal clusters of MOFs can pave the way to realize superior H_2 storage materials by offering high Pd loadings and their homogeneous distribution while preserving high surface area and pore volume. These materials could also enable precise investigation of the guest-Pd interaction both experimentally and computationally by taking advantage of highly crystalline and well-defined MOF structure. The incorporation of precisely positioned Pd-OMSs into the MOFs, however, still remains highly challenging. Here, we report on the synthesis of MOFs with surface areas up to 1494 m^2 g^{-1} possessing Pd–Cu paddle wheel units by simply reacting $PdCu(AcO)_4H_2O$ with tritopic organic linkers at room temperature (Fig. 1). The resulting MOFs were found to possess nearly 1 : 1 metal ratio (Pd : Cu) with precisely controlled positions by using the predesigned metal clusters. The incorporation of Pd single atoms in the form of OMSs led to an enhanced affinity towards H_2 leading to the Q_{st} values up to 8.9 kJ mol^{-1}.

The synthesis of $PdCu(AcO)_4H_2O$ was achieved *via* the dissolution of $Pd_3(AcO)_6$ and $Cu(AcO)_2{\cdot}2H_2O$ in a mixture of acetic acid/H_2O at 85 °C for 3 h, followed by recrystallization at 6 °C for 3 days. The resulting complex, $\{PdCu(AcO)_4H_2O(AcO)_2\}_n$, formed a superstructure, in which $PdCu(AcO)_4H_2O$ paddle

[a] *Graduate School of EEWS, Korea Advanced Institute of Science and Technology (KAIST), 373-1 Guesong Dong, Daejeon, 305-701, Republic of Korea*
[b] *Department of Chemistry, University of Fribourg, Fribourg 1700, Switzerland. E-mail: ali.coskun@unifr.ch*
[c] *NIST Center for Neutron Research, National Institute of Standards and Technology, Gaithersburg, Maryland 20899-6102, USA. E-mail: taner@nist.gov*

† Electronic supplementary information (ESI) available: Materials, synthesis method, XRD, XPS, gas adsorption result and so on. See DOI: 10.1039/c8cc04661a

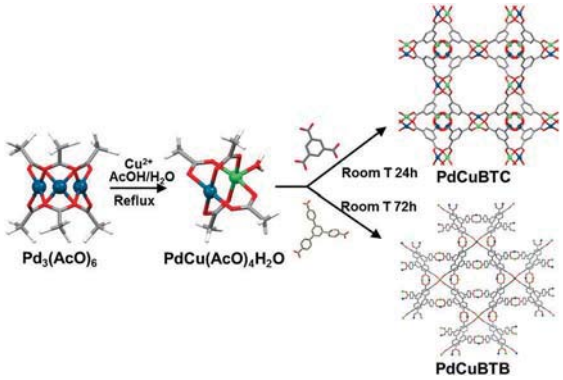

Fig. 1 Synthetic strategy for the preparation of bimetallic MOFs incorporating pre-designed Pd–Cu paddle wheel units with precisely controlled metal positions and ratios.

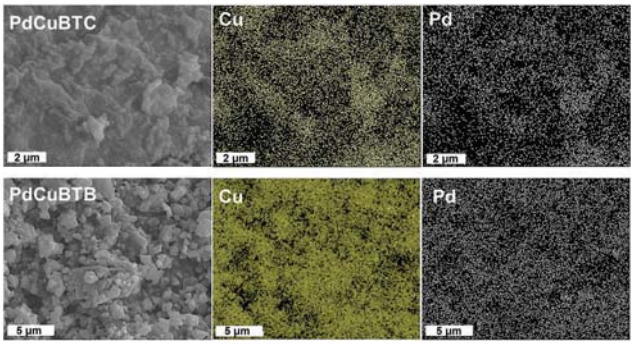

Fig. 3 Energy dispersive spectroscopy (EDS) mapping of PdCuBTC (top) and PdCuBTB (bottom) crystals synthesized by using pre-designed $PdCu(AcO)_4H_2O$ and organic linkers.

wheel units were linked through hydrogen bonding interactions between coordinated water molecules located on the Cu sites and excess acetic acid molecules.[26] The powder X-ray diffraction (XRD) and Fourier transform infrared (FT-IR) spectra of the Pd–Cu acetate were in a good agreement with the earlier report (Fig. 1 and Fig. S1, ESI†), thus confirming its successful formation. We would like to note that the impurities such as Pd nanoparticles formed during the synthesis of $Pd_3(AcO)_6$ should be excluded through recrystallization prior to its use to prevent the incorporation of Pd nanoparticles into the resulting MOFs. Two different PdCu MOFs possessing similar structures to those of Cu_3BTC_2(MOF-199, HKUST-1)[27] and Cu_3BTB_2 (MOF-14)[28] were obtained by simply mixing $PdCu(AcO)_4H_2O$ and organic linkers, which are benzene-1,3,5-tricarboxylic acid (BTC) and 1,3,5-tris(4-carboxyphenyl)benzene (BTB) in the solvent mixture of DMF/EtOH/H_2O at room temperature. Detailed synthesis procedure is described in the ESI.† The XRD and FT-IR spectra of both PdCuBTC and PdCuBTB matched well with their Cu analogues, MOF-199[27] and MOF-14,[28] respectively (Fig. 2 and Fig. S3, ESI†). The successful synthesis of two different MOFs by simply varying the size of the organic linker points to the versatile usage of $PdCu(AcO)_4H_2O$ for the synthesis of various MOFs incorporating Pd–Cu paddle wheel units.

In order to observe the morphology of bimetallic MOFs, we have performed scanning electron microscopy (SEM) analyses. SEM images of the PdCuBTC and PdCuBTB showed the formation of crystalline particles (Fig. 3 and Fig. S2, ESI†). PdCuBTC revealed much smaller particle sizes (<100 nm) compared to PdCuBTB

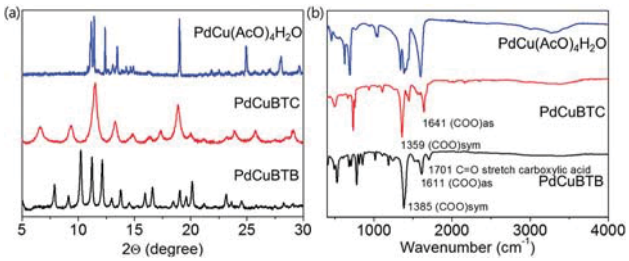

Fig. 2 (a) XRD and (b) FT-IR spectra of $PdCu(AcO)_4H_2O$ complex and as-synthesized PdCu MOFs, namely PdCuBTC and PdCuBTB.

(~300 nm), which is attributed to the high and low solubility of BTC and BTB linkers in the reaction solvents, respectively. Noticeably the smaller particle size of PdCuBTC resulted in the broadening of XRD peaks compared to that of Cu_3BTC_2 (Fig. S3, ESI†). Also, we attribute the lack of morphology control to the stirring applied during the synthesis. Energy dispersive spectroscopy (EDS) mapping of Cu and Pd ions of PdCuBTC and PdCuBTB crystals showed homogeneous distribution of both Pd and Cu, thus confirming the successful incorporation of Pd and Cu OMSs into the MOF structures. Notably, the important aspect of this approach is that the ratio Pd and Cu in $PdCu(AcO)_4H_2O$ was maintained in the final MOF structures, thus allowing strict control over the metal ratios and positions. The ratios of Pd and Cu in $PdCu(AcO)_4H_2O$ and PdCu MOFs were analysed *via* X-ray photoelectron spectroscopy analysis. $PdCu(AcO)_4H_2O$ showed the Pd/Cu molar composition of 50.3/49.7, thus confirming the successful formation of Pd–Cu paddle wheel unit. In addition, we also observed Pd/Cu molar ratios of 50.1/49.9 and 53.5/46.5 for the PdCuBTC and PdCuBTB, respectively, also an indication for the successful incorporation of Pd–Cu paddle wheel units into the resulting MOF structures. Also, inductively coupled plasma atomic emission spectroscopy (ICP-AES) and EDS analysis revealed nearly equimolar composition of Pd and Cu in both MOFs, thus confirming the successful incorporation of Pd–Cu paddle wheel units into the resulting MOFs (Tables S1 and S2, ESI†).

During the synthesis of PdCu MOFs, we observed immediate formation of a dark-green precipitate when the transparent solutions of $PdCu(AcO)_4H_2O$ and organic linkers were mixed, which eventually became light-green over the course of the reaction (1 and 3 days for PdCuBTC and PdCuBTB, respectively). The understanding of this observation can elucidate the reason for the retention of metal ratio during the MOF synthesis. Accordingly, we have investigated structural changes during the synthesis of MOFs using XRD (Fig. S4a, ESI†). XRD analysis of dark-green powder revealed new crystalline peaks different from those of $PdCu(AcO)_4H_2O$, indicating the formation of an intermediate phase. After stirring for 3 days, we observed the diffraction patterns corresponding to PdCuBTB. Importantly, the 2Θ value of the first peak shifted towards lower angles during the synthesis: 11.1, 5.8, 4.6° for $PdCu(AcO)_4H_2O$, intermediate phase and PdCuBTB, respectively, mainly due to an increase in unit

cell dimensions. We further investigated the chemical changes using FT-IR (Fig. S4b, ESI†). $PdCu(AcO)_4H_2O$ revealed a relatively simple spectrum featuring symmetric and asymmetric stretching vibration modes at 1385 and 1597 cm^{-1}, respectively, which are assigned to the CH_3COO^- of the Pd–Cu paddle wheel unit. The FT-IR spectrum became more complicated in the intermediate phase, which is relatively similar to that of PdCuBTB. As the intermediate phase formed, the appearance of C=O, $(COO)_{sym}$ and $(COO)_{as}$ vibration peaks at 1688, 1392 and 1601 cm^{-1} were observed along with a significant change in the entire spectrum, which can be attributed to the ligand exchange from small acetic acid to the bulky BTB linker. Based on these observations, we proposed that the formation of PdCu MOFs using predesigned bimetallic Pd–Cu paddle wheel units involves relatively mild exchange of the acetic acid moieties bonded to the Pd–Cu paddle wheel unit with tritopic linkers such as BTC and BTB due to their higher acidity. As this exchange process does not involve the dissociation of metal clusters, it enables the homogeneous distribution of two different metals within the MOF structure with high precision.

The unique bimetallic structure of MOFs also led to peculiar chemical states of metal ions in Pd–Cu paddle wheel units. The chemical states of Pd and Cu ions in $Pd_3(AcO)_6$, $PdCu(AcO)_4H_2O$, PdCuBTC and PdCuBTB have been investigated (Fig. S5, ESI†) using XPS. The Pd_{3d} XPS spectra of all the samples showed narrow double peaks with binding energies located at 337.1 and 342.5 eV assigned to Pd^{2+}, thus confirming the incorporation of Pd ions into the paddle wheel units of MOFs. Contrary to the previous report by Fischer *et al.*,[29] in which PdCuBTC revealed the incorporation of both Pd nanoparticles and Pd^{2+} into the framework, our approach excluded the formation of Pd nanoparticles, thus enabling the incorporation of single atom Pd OMSs into MOFs. This result is attributed to the mild reaction temperature in our synthesis, room *T vs. ca.* 120 or 90 °C, prohibiting the formation of Pd or PdO nanoparticles. In order to confirm the absence of Pd or PdO nanoparticles within the MOF crystals, we have analysed the diffraction pattern of PdCuBTB at 2Θ range from 32 to 42°. Notably, the diffraction peaks originating from (101) plane of PdO and (111) plane of Pd nanoparticles were not observed (Fig. S6, ESI†), thus verifying our conclusion. Furthermore, Cu_{2P} XPS spectra revealed unique chemical states (Fig. S5, ESI†). Pd–Cu paddle wheel revealed the combination of Cu^{1+} and Cu^{2+}. Noticeably, the ratio of Cu^{1+} and Cu^{2+} varied depending on the type of organic linkers: $PdCu(AcO)_4H_2O$ (36.6 : 63.4), PdCuBTC (27.1 : 72.9) and PdCuBTB (57.6 : 42.4). Notably, these findings are in good agreement with the previously reported examples of $Cu_3(BTC)_2(H_2O)_3$, which also showed the coexistence of Cu^{1+} and Cu^{2+} within the paddle wheel units. The reduction of Cu^{2+} to Cu^{1+} was attributed to the thermal activation step to remove coordinated solvent molecules occupying axial sites on each Cu^{2+} ion. This redox phenomenon was suggested to originate from the partial and reversible opening of the paddle wheel units.[30–32] However, we also do not rule out the possibility of missing organic linkers as the origin of Cu^{1+} species.

The pore characteristics of PdCuBTC and PdCuBTB were investigated by Ar adsorption–desorption isotherms measured at 87 K (Fig. 4a). Both PdCuBTC and PdCuBTB revealed predominantly

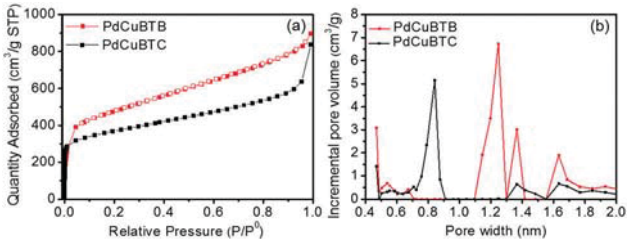

Fig. 4 (a) Ar adsorption–desorption isotherms and (b) micropore size distribution of PdCuBTC and PdCuBTB.

type I isotherms indicating the presence of well-developed micropores with the surface areas of 1175 and 1494 $m^2\ g^{-1}$, respectively. Notably, we also observed the characteristics of type II isotherms at high partial pressures, which is indicative of a measurable external surface area originating from interparticle meso/macropores. In order to analyze the pore structure of MOFs, Density Functional Theory (DFT) pore size distribution analyses were conducted (Fig. 4b). While PdCuBTC revealed two peaks centered at 4 and 8 Å, PdCuBTB showed a peak at 4 Å along with multiple peaks ranging from 11 to 17 Å, which are in good agreement with those of MOF-199[27] and MOF-14.[28]

In order to probe the effect of Pd OMSs on the affinity of H_2 towards bimetallic MOFs, we have measured (Fig. 5a and b) H_2 isotherms up to 1.3 bar at 67, 77 and 87 K.[33] PdCuBTC and PdCuBTB showed H_2 uptake capacity of 2.6 and 2.9 wt%, respectively at 67 K and decreased as the temperature increased to 87 K. Heats of adsorption (Q_{st}) values for H_2 were calculated from the H_2 isotherms (Fig. 5c). While it is well-known that Q_{st} of Cu_3BTC_2 for H_2 rarely decreases until the complete saturation of OMSs,[34] we observed Q_{st} value of 7.2 and 8.9 kJ mol^{-1} for PdCuBTC and PdCuBTB, respectively at zero coverage and it gradually decreased with increasing H_2 loading and eventually became ~5 kJ mol^{-1} at high loading. We suggest that the incomplete activation of PdCuBTC as evidenced from its lower Cu^{1+} content as well as residual coordinated H_2O molecules (Fig. S7, ESI†) led to lower Q_{st} compared to that of PdCuBTB. Enhanced Q_{st} values at low pressure compared to the simple Cu paddle wheel units in both Cu_3BTC_2 and Cu_3BTB_2 clearly demonstrate the effect of Pd OMSs on the superior H_2 binding. We attribute the lower H_2 Q_{st} at higher loading to the presence of meso/macropores in the MOFs. This result also matches well with the previous report by Sumby and Doonan,[24] which also showed enhanced Q_{st} values in the range of 8.6–10 kJ mol^{-1} for H_2 in their metal–organic polyhedras composed of Pd–Cu paddle wheel units.

In order to elucidate the effect of the strong H_2 binding at room temperature H_2 storage capacity (Fig. 5a and b), we conducted H_2 adsorption/desorption measurement at 298 K, which showed irreversible chemisorption such that the adsorbed hydrogen molecules did not come back even after heating the sample to 100 °C. The second H_2 isotherm of PdCuBTC at 298 K showed almost no adsorption, confirming that the first adsorption was irreversible and collapsed sample (Fig. 5a). Importantly, TCD analysis did not show any H_2 desorption, thus further proving irreversible adsorption and/or chemical reaction, that is thermally activated near room temperature.

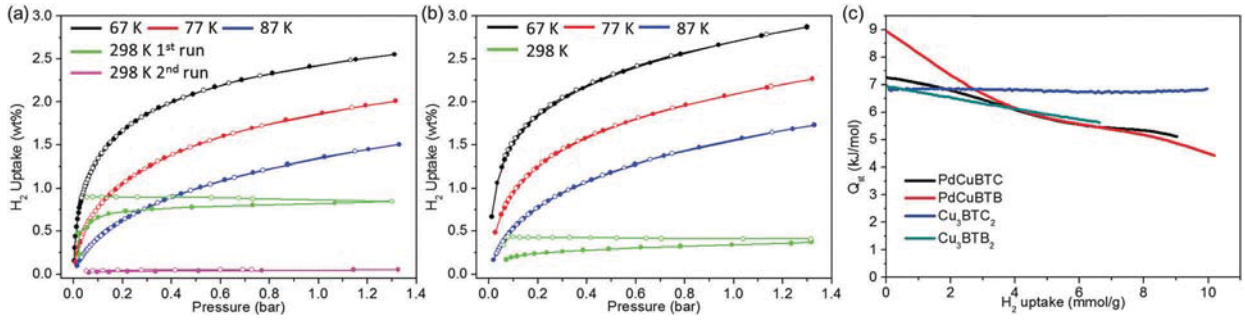

Fig. 5 H_2 adsorption and desorption isotherms of (a) PdCuBTC and (b) PdCuBTB at 67, 77 and 87 K. (c) Isosteric heats of adsorption (Q_{st}) values of PdCuBTC and PdCuBTB for H_2 as a function of its absolute loading. The Q_{st} values were calculated using H_2 adsorption data at 67, 77 and 87 K using the Clausius–Clapeyron equation. Blue dotted line indicates the Q_{st} of H_2 for Cu_3BTC_2.

Negligible N_2 adsorption of the MOFs after the H_2 uptake experiment at 298 K points to the degradation of framework structure, which is also visually verified by the fact that the sample color turned from light green to black (Fig. S9 and S10, ESI†) FT-IR spectra of PdCuBTC showed both $(COO^-)_{as}$ and C═O peak at 1611 and 1701 cm^{-1}, respectively (Fig. S11, ESI†), thus indicating the partial hydrogenation COO^- of BTC and the reduction of Pd and resulting in the collapse of MOF structure, which might be attributed to the dissociative adsorption of H_2 to the Pd OMSs facilitated by the densely located Pd/Cu paddle wheel units at 298 K.

In conclusion, we demonstrated successful synthesis of two bimetallic, high surface area, MOF structures incorporating Pd–Cu paddle wheel units under mild reaction conditions. The analysis of Pd–Cu MOFs revealed nearly 1 : 1 metal ratio of Pd and Cu and their homogeneous distribution, thus inheriting the atomic-level order of predesigned Pd–Cu metal cluster. The positive effect of Pd incorporation on H_2 affinity was clearly probed with increased Q_{st} values. In a broader context, the precise positioning of metal centers in multimetal MOFs could certainly help to fully understand the origin of gas affinity and reactivity in these systems, thus contributing to the design of new sorbents with fully controlled/understood functions.

We acknowledge the support from the Swiss National Science Foundation (SNF) for funding of this research (200021-175947).

Conflicts of interest

There are no conflicts to declare.

References

1 G. Ferey, *Chem. Soc. Rev.*, 2008, **37**, 191–214.
2 H.-C. Zhou, J. R. Long and O. Yaghi, *Chem. Rev.*, 2012, **112**, 673–674.
3 M. Eddaoudi, J. Kim, N. Rosi, D. Vodak, J. Wachter, M. O'Keeffe and O. M. Yaghi, *Science*, 2002, **295**, 469–472.
4 P. Z. Li, X. J. Wang, S. Y. Tan, C. Y. Ang, H. Z. Chen, J. Liu, R. Q. Zou and Y. L. Zhao, *Angew. Chem., Int. Ed.*, 2015, **54**, 12748–12752.
5 A. Cadiau, K. Adil, P. M. Bhatt, Y. Belmabkhout and M. Eddaoudi, *Science*, 2016, **353**, 137–140.
6 D. Kim and A. Coskun, *Angew. Chem., Int. Ed.*, 2017, **56**, 5071–5076.
7 J. Lee, O. K. Farha, J. Roberts, K. A. Scheidt, S. T. Nguyen and J. T. Hupp, *Chem. Soc. Rev.*, 2009, **38**, 1450–1459.
8 D. Kim, D. W. Kim, O. Buyukcakir, M.-K. Kim, K. Polychronopoulou and A. Coskun, *Adv. Funct. Mater.*, 2017, 1700706.
9 R. J. Comito, K. J. Fritzsching, B. J. Sundell, K. Schmidt-Rohr and M. Dincă, *J. Am. Chem. Soc.*, 2016, **138**, 10232–10237.
10 C. B. He, K. D. Lu, D. M. Liu and W. B. Lin, *J. Am. Chem. Soc.*, 2014, **136**, 5181–5184.
11 K. Liang, J. J. Richardson, J. Cui, F. Caruso, C. J. Doonan and P. Falcaro, *Adv. Mater.*, 2016, **28**, 7910–7914.
12 L. E. Kreno, K. Leong, O. K. Farha, M. Allendorf, R. P. Van Duyne and J. T. Hupp, *Chem. Rev.*, 2012, **112**, 1105–1125.
13 Y. Li, S. S. Zhang and D. T. Song, *Angew. Chem., Int. Ed.*, 2013, **52**, 710–713.
14 F. Wang, W. Liu, S. J. Teat, F. Xu, H. Wang, X. Wang, L. An and J. Li, *Chem. Commun.*, 2016, **52**, 10249–10252.
15 M. Hu, J. Reboul, S. Furukawa, L. Radhakrishnan, Y. Zhang, P. Srinivasu, H. Iwai, H. Wang, Y. Nemoto, N. Suzuki, S. Kitagawa and Y. Yamauchi, *Chem. Commun.*, 2011, **47**, 8124–8126.
16 J. Tang and Y. Yamauchi, *Nat. Chem.*, 2016, **8**, 638–639.
17 A. Dhakshinamoorthy and H. Garcia, *Chem. Soc. Rev.*, 2012, **41**, 5262–5284.
18 J. Yu, C. Mu, B. Yan, X. Qin, C. Shen, H. Xue and H. Pang, *Mater. Horiz.*, 2017, **4**, 557–569.
19 P. Falcaro, R. Ricco, A. Yazdi, I. Imaz, S. Furukawa, D. Maspoch, R. Ameloot, J. D. Evans and C. J. Doonan, *Coord. Chem. Rev.*, 2016, **307**, 237–254.
20 M. Sabo, A. Henschel, H. Froede, E. Klemm and S. Kaskel, *J. Mater. Chem.*, 2007, **17**, 3827–3832.
21 Y. E. Cheon and M. P. Suh, *Angew. Chem., Int. Ed.*, 2009, **48**, 2899–2903.
22 C. Zlotea, R. Campesi, F. Cuevas, E. Leroy, P. Dibandjo, C. Volkringer, T. Loiseau, G. Ferey and M. Latroche, *J. Am. Chem. Soc.*, 2010, **132**, 2991–2997.
23 G. Li, H. Kobayashi, J. M. Taylor, R. Ikeda, Y. Kubota, K. Kato, M. Takata, T. Yamamoto, S. Toh, S. Matsumura and H. Kitagawa, *Nat. Mater.*, 2014, **13**, 802–806.
24 J. M. Teo, C. J. Coghlan, J. D. Evans, E. Tsivion, M. Head-Gordon, C. J. Sumby and C. J. Doonan, *Chem. Commun.*, 2016, **52**, 276–279.
25 S. Wongsakulphasatch, F. Nouar, J. Rodriguez, L. Scott, C. L. Guillouzer, T. Devic, P. Horcajada, J.-M. Grenèche, P. L. Llewellyn, A. Vimont, G. Clet, M. Daturi and C. Serre, *Chem. Commun.*, 2015, **51**, 10194–10197.
26 N. S. Akhmadullina, N. V. Cherkashina, N. Y. Kozitsyna, I. P. Stolarov, E. V. Perova, A. E. Gekhman, S. E. Nefedov, M. N. Vargaftik and I. I. Moiseev, *Inorg. Chim. Acta*, 2009, **362**, 1943–1951.
27 S. S.-Y. Chui, S. M.-F. Lo, J. P. H. Charmant, A. G. Orpen and I. D. Williams, *Science*, 1999, **283**, 1148–1150.
28 B. Chen, M. Eddaoudi, S. T. Hyde, M. O'Keeffe and O. M. Yaghi, *Science*, 2001, **291**, 1021–1023.
29 W. Zhang, Z. Chen, M. Al-Naji, P. Guo, S. Cwik, O. Halbherr, Y. Wang, M. Muhler, N. Wilde, R. Gläser and R. A. Fischer, *Dalton Trans.*, 2016, **45**, 14883–14887.
30 J. Szanyi, M. Daturi, G. Clet, D. R. Baer and C. H. F. Peden, *Phys. Chem. Chem. Phys.*, 2012, **14**, 4383–4390.
31 N. Nijem, H. Bluhm, M. L. Ng, M. Kunz, S. R. Leone and M. K. Gilles, *Chem. Commun.*, 2014, **50**, 10144–10147.
32 A. S. Duke, E. A. Dolgopolova, R. P. Galhenage, S. C. Ammal, A. Heyden, M. D. Smith, D. A. Chen and N. B. Shustova, *J. Phys. Chem. C*, 2015, **119**, 27457–27466.
33 I. Eryazici, J. T. Hupp, O. K. Farha and T. Yildirim, *J. Am. Chem. Soc.*, 2013, **135**, 11887–11894.
34 H. Du, J. Bai, C. Zuo, Z. Xin and J. Hu, *CrystEngComm*, 2011, **13**, 3314–3316.